Quantifying day-to-day variations in 4DCBCT-based PCA motion models

Salam Dhou[1], John Lewis[2*], Weixing Cai[3], Dan Ionascu[4], and Christopher Williams[5*]

[1] American University of Sharjah, Sharjah, United Arab Emirates

[2] Cedars Sinai Medical Center, Los Angeles, CA 90048, United States of America

[3] Memorial Sloan Kettering Cancer Center, New York, NY 10065, United States of America

[4] University of Cincinnati, Cincinnati, OH 45267, United States of America

[5] Brigham and Women's Hospital, Dana-Farber Cancer Institute, and Harvard Medical School, Boston, MA 02115, United States of America

[*]Both authors contributed equally to this work

E-mail: sdhou@aus.edu, jlewisphysics@gmail.com

Abstract: The aim of this paper is to quantify the day-to-day variations of motion models derived from pre-treatment 4-dimensional cone beam CT (4DCBCT) fractions for lung cancer stereotactic body radiotherapy (SBRT) patients. Motion models are built by 1) applying deformable image registration (DIR) on each 4DCBCT image with respect to a reference image from that day, resulting in a set of displacement vector fields (DVFs), and 2) applying principal component analysis (PCA) on the DVFs to obtain principal components representing a motion model. Variations were quantified by comparing the PCA eigenvectors of the motion model built from the first day of treatment to the corresponding eigenvectors of the other motion models built from each successive day of treatment. Three metrics were used to quantify the variations: root mean squared (RMS) difference in the vectors, directional similarity, and an introduced metric called the Euclidean Model Norm (EMN). EMN quantifies the degree to which a motion model derived from the first fraction can represent the motion models of subsequent fractions. Twenty-one 4DCBCT scans from five SBRT patient treatments were used in this retrospective study. Experimental results demonstrated that the first two eigenvectors of motion models across all fractions have smaller RMS (0.00017), larger directional similarity (0.528), and larger EMN (0.678) than the last three eigenvectors (RMS: 0.00025, directional similarity: 0.041, and EMN: 0.212). The study concluded that, while the motion model eigenvectors varied from fraction to fraction, the first few eigenvectors were shown to be more stable across treatment fractions than others. This supports the notion that a pre-treatment motion model built from the first few PCA eigenvectors may remain valid throughout a treatment course. Future work is necessary to quantify how day-to-day variations in these models will affect motion reconstruction accuracy for specific clinical tasks.

Keywords: Four-dimensional cone beam CT (4DCBCT), PCA motion model, stereotactic body radiation therapy (SBRT), inter-fraction variations.

1. Introduction

Motion modeling is a technique that uses prior information to enable the reconstruction of a full three-dimensional (3D) image based on limited information. In radiation therapy, this technique has been demonstrated as a potentially useful way to reconstruct 3D computed tomography (CT) scans based on

single planar kV images or using respiratory motion surrogates. The resultant 3D images can then be used to identify any aberrant patient motion and to calculate delivered dose. This technique has particular utility in hypo-fractionated treatments such as stereotactic body radiotherapy (SBRT) in which a few large doses of radiation are delivered to small, well-defined tumors [1].

SBRT has been used successfully to treat early-stage non-small cell lung cancer, however, respiratory motion can be a cause of uncertainty in localizing the tumor and other organs during radiotherapy delivery, potentially compromising the effectiveness of the therapy. Uncertainties caused by respiration can affect the accuracy of imaging, treatment planning, and treatment delivery [2]. Respiratory motion modeling techniques have been developed to address these respiratory-induced uncertainties by enabling the estimation of the locations of lesions and anatomical structures in 3D at all times throughout treatment [3]–[8], enabling clinicians to assess the impact of motion during therapy.

Planning for SBRT is typically performed using 4-dimesional CT (4DCT) images, which are often captured days or weeks before treatment. In many motion modeling approaches, these planning images are used for building patient-specific motion models [5], [8]–[11]. These models are often generated by applying principal component analysis (PCA) to a set of deformation vector fields (DVFs) between the phases of the 4DCT. The first few PCA eigenvectors, which describe most of the variance in the 4DCT, serve as the motion model.

One potential issue of using pre-treatment planning imaging to generate motion models is the applicability of these models at the time of treatment. A patient's anatomy or respiratory pattern may change in the intervening time, and thus, motion models built using the planning 4DCT may not reliably represent patient anatomy and/or organ motion at the time of treatment delivery [12]. In fractionated SBRT, radiotherapy treatment is delivered in a few fractions (typically 3 to 5), and it is possible that no single motion model may reliably and adequately represent the patient motion and anatomy on each day of treatment, limiting the clinical utility of a technique based on a planning 4DCT-derived model. This may make it necessary to generate motion models at the time of each treatment fraction.

Onboard image guidance techniques available in the treatment room, such as cone-beam CT (CBCT), can obtain patient images in the treatment position immediately before and/or after treatment, making CBCT particularly well-suited for image-guided radiotherapy. The development of 4-dimensional CBCT has further allowed the changes in a patient's anatomy due to respiratory motion to be imaged at the time of treatment. These 4DCBCT scans can be reconstructed by sorting projection images into phases by extracting a respiratory signal and reconstructing each set of projections into separate 3D images [13]–[16].

4DCBCT images are acquired immediately before treatment when the patient is in treatment position. Building motion models based on 4DCBCT images has the potential to resolve problems with inter-fraction organ motion or changes in respiratory patterns which could therefore help in reducing modeling uncertainties [17], [18]. However, the 4DCBCT images being used to build the motion model may contain artifacts due to the small number of projections used for the image reconstruction at each respiratory phase [19]–[24]. Thus, the quality of 4DCBCT images may presents a significant challenge when using them in building motion models.

This paper aims to quantify and discuss the inter-fraction variations of PCA-based motion models built from 4DCBCT images captured immediately prior to each fraction of a radiotherapy treatment course. This analysis method can be applied to any motion model involving displacement vectors, not only the specific PCA motion model studied in this paper. Several studies have explored the changes in patient

anatomy and motion patterns over the course of fractionated radiotherapy [25]–[29].These studies showed that safety margins added to account for respiratory motion may not be adequate if they are based on a single imaging session, especially when relying on external or internal surrogate motion. They also showed that margins for lung targets should include inter-fraction variations in breathing. Several works investigated the inter-fraction variations over a course of radiotherapy treatment for lung cancer [1], [30]–[32]. Matsugi et al. studied the day-to-day variations in the gross tumor volume (GTV), position, and motion range over a course of radiotherapy for lung cancer using 4DCT. Their study found that there are small day-to-day variations in GTV, position, and motion range which may require additional assessment to the size of the inferred safety margins [1]. Using 4DCBCT, Sonke et al. quantified the day-to-day variability in lung tumor trajectory and mean position during a radiotherapy treatment course [30]. Their study showed that tumor trajectory shape and baseline variations can be accurately monitored using 4DCBCT which can help develop image-guided strategies for motion correction to reduce safety treatment margins [30]. Rit et al. have also studied the day-to-day variability of the diaphragm motion throughout a radiotherapy treatment course of lung cancer and its effect on safety margins [31]. Their study showed that the diaphragm position and the intra-acquisition variability have a limited impact on dose distributions and derived safe margins.

As discussed, day-to-day variations in the motion patterns of the tumor or other individual anatomical structures during the course of radiation therapy have been studied in the literature, but the relationship between these variations and their effect on the validity of a pre-treatment motion model have not been established. This work aims to quantify these variations and study their effect on the validity of a pre-treatment motion model built from 4DCBCT-based images captured prior to the first fraction of a radiotherapy treatment course. A preliminary version of this work has been reported [32].

The manuscript is organized as follows: Section 2 describes the materials and the methods used to generate the fraction-specific motion models and the evaluation criteria. Section 3 presents the experimental results. Section 4 discusses the results. Section 5 concludes the paper.

2. Materials and methods

2.A. Data acquisition

Twenty-one 4DCBCT scans from five SBRT patient treatments acquired using the Elekta Synergy system (Elekta Oncology Systems Ltd., Crawley, West Sussex, UK) were used retrospectively in this study. Projection images were acquired at 5.5 fps for 4 min over an arc of 200 degrees to optimize the sampling for 4DCBCT. Each patient dataset has between 3 and 5 fraction scans with a total of 1304 to 1356 projections in each scan. To produce the 4DCBCT images, respiratory signals from each scan have been extracted using Amsterdam Shroud method [10], [13] and used to sort the scan projections into six phase bins. Projections at each phase bin were reconstructed independently to produce six 4DCBCT images for each scan using the Feldkamp, Davis and Kress (FDK) reconstruction algorithm [33] implemented in the Reconstruction ToolKit (RTK) [34].

2.B. Principal Component Analysis (PCA) for motion modeling

Building PCA motion models from a set of 4DCBCT images captured at each fraction requires performing the following two steps:

1) Applying deformable image registration (DIR) on each 4DCBCT image from the dataset of each fraction with respect to a reference image chosen from that set. In this study, the first image was chosen as a reference image where the respiratory phase was peak exhale. DIR finds the displacement between each voxel of the reference image and its correspondence in each other image in the set. This will result in displacement vector fields (DVFs) representing the voxel-wise displacements between the reference image and all other images of the set. The Demons algorithm was used in this study with double force implementation [35].
2) Performing dimensionality reduction using PCA on the DVFs. This step takes a high-dimensional DVF dataset and enables it to be represented using only a few parameters. PCA determines a new set of basis eigenvectors that span the subspace defined by the set of DVFs by finding the directions of maximum variance. Dimensionality can be reduced by discarding basis vectors which explain negligible parts of the total overall variance. Thus, PCA results in a smaller subspace spanned by a set of basis eigenvectors that capture the largest modes of variance in the DVFs. A PCA motion model is defined by a linear combination of a few basis eigenvectors and weighting parameters (2-3), known as PCA coefficients [4], [36]. Using this definition, the DVF can be represented as [5], [37]:

$$\mathbf{DVF} = \overline{\mathbf{DVF}} + \sum_{m=1}^{M} u_m w_m(t) \qquad (1)$$

where $\overline{\mathbf{DVF}}$ is the mean DVF. $\boldsymbol{u_m}$ are the eigenvectors obtained from PCA and are defined in space, while the parameters $\boldsymbol{w_m(t)}$ are PCA coefficients and are defined in time. *M* is the number of eigenmodes.

2.C. Evaluation of the day-to-day variations in motion models

The following criteria comprising of three metrics is used to evaluate and compare motion models built from different fractions.

2.C.a. Evaluation Metrics

1) **Root mean square (RMS) difference between the eigenvectors of the motion model derived from the reference fraction and the corresponding eigenvectors of the motion models derived from subsequent fractions.** The RMS measures the absolute differences between the corresponding normalized eigenvectors. It is computed by finding the square root of the mean square difference between the compared eigenvectors as follows:

$$\boldsymbol{RMS} = \sqrt{\frac{\sum_{n=1}^{N}(\boldsymbol{v_{1,m,n}} - \boldsymbol{v_{f,m,n}})^2}{\boldsymbol{N}}} \qquad (2)$$

where $\boldsymbol{v}_{1,m,n}$ corresponds to the n^{th} element in the eigenvector in the first fraction of treatment (reference fraction)**,** and $\boldsymbol{v}_{f,m,n}$corresponds to the n^{th} element in the eigenvector in the f^{th} fraction of treatment. m is the eigenmode and *N* is the number of elements in the eigenvectors.

2) **Directional similarity of the eigenvectors of the motion model derived from the reference fraction and the corresponding eigenvectors of the motion models derived from subsequent fractions.** The directional similarity is computed by finding the dot product between the compared eigenvectors. The dot product is the directional multiplication between vectors. It used in this study as a measure of the projection of one eigenvector onto another which can find how much the vectors vary in direction. If two compared

eigenvectors are pointing in the same direction, their dot product will result in 1. It will result in zero if they are perpendicular, and -1 if they are pointing in opposite directions. In this study, the dot product is computed for eigenvectors of the motion model of the first fraction, as the reference fraction, and the corresponding eigenvectors in the subsequent fractions to quantify their directional similarity.

3) **Euclidean Model Norm (EMN) defined as the Euclidean norm of each eigenvector in the basis formed by the set of the first three eigenvectors in the reference fraction.** This quantity is defined to represent how well an eigenvector can be reconstructed using a motion model built using the first three eigenvectors from the motion model of the first day of treatment. This metric is introduced to account for the fact that even though the eigenvectors of the motion may change day-to-day, the model formed by a subset of these vectors from a prior day may still be able to represent the motion on a subsequent day. EMN is defined as:

$$EMN_{f,m} = \sqrt{\sum_{k=1}^{K} \left| v_{1,k} \cdot v_{f,m} \right|^2} \qquad (3)$$

where $v_{1,k}$ is the eigenvector from the first fraction at the k^{th} eigenmode and $v_{f,m}$ is the eigenvector from the f^{th} fraction at the m^{th} eigenmode. The eigenvectors used are all normalized to unit length and K is the number of eigenmodes used to define the reference-day motion model. In this study we have selected K = 3. Previous studies showed that the organ motion measured by the DVFs can be represented by a linear combination of only a few (2–3) PCA basis eigenvectors and coefficients [4], [36]. Thus, using EMN, we want to find quantitatively the degree to which such a motion model built from the first three eigenvectors from the first fraction can represent other eigenvectors from subsequent fractions. The EMN is calculated as the square root of the sum of the squares of the dot products of the reference model eigenvectors and other eigenvectors from subsequent fractions. An EMN of unity would reflect that an eigenvector is completely represented in a motion model derived from the first fraction, whereas an EMN of zero would indicate that the motion captured by a particular eigenvector would not be captured in that motion model. The EMN, equation (3), has been used as a global measure of quantifying day-to-day variations among different motion models formed by the first three eigenvectors of the first fraction showing the most variances of the dataset. This criteria is relevant if the eigenvectors of the first fraction are different than the eigenvectors from later fractions, but cover a similar range of possible motion combinations (i.e., span the same subspace). For example, if eigenvector 1 and eigenvector 2 switch places between fractions, these criteria reflect that the motion models would be equivalent.

2.C.b. Alignment

The evaluation criteria discussed above are applied on the datasets under two alignment cases:

Alignment #1: Rigid registration according to bony anatomy is applied to register the entire 4DCBCT images in the subsequent fractions to the entire images in the first fraction.

Alignment #2: Rigid registration according to a region of interest (ROI) around the tumor is applied to register the entire 4DCBCT images in the subsequent fractions to the corresponding ROI in the images in the first fraction.

This alignment procedure is performed to avoid bias due to mis-registration of the images, and simulates the clinical practices of either aligning to bony anatomy (Alignment #1) or the target (Alignment #2).

3. Experimental results

In this section, the day-to-day variations of motion models derived from several treatment fractions are evaluated on patient datasets according to the evaluation criteria proposed in Section 2.C. Figure 1 shows the first three eigenvectors of the PCA motion model obtained from the first fraction of Patient #1. The PCA eigenvectors are plotted on a coronal slice from that dataset. In this figure, the eigenvectors are normalized but not scaled. The vector's length and direction correspond to the magnitude and direction of its motion, respectively. The first PCA eigenvector in (a) show a superior-inferior motion, while the second and third eigenvectors in (b) and (c), respectively show a combination of left-right (LR) and anterior-posterior (AP) motion.

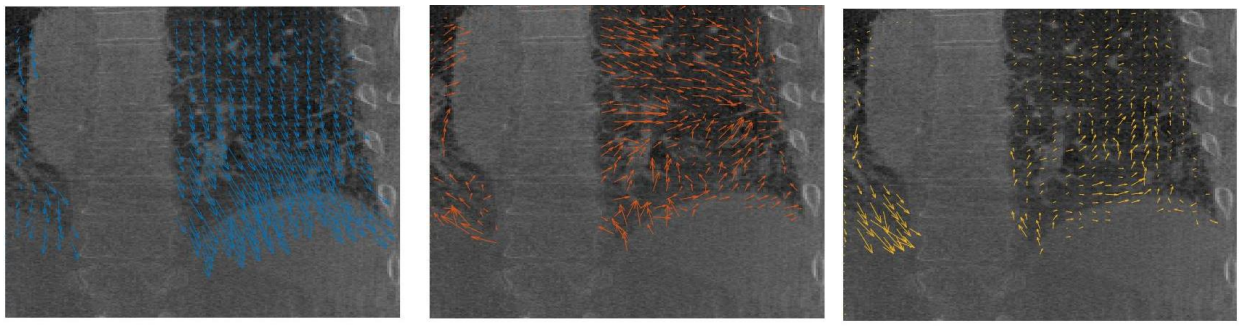

(a) (b) (c)

Figure 1: PCA eigenvectors for Patient #1 at Fraction #1 for the eigenmodes (a) 1, (b) 2, and (c) 3.

Figure 2 (a) shows the spectrum of the eigenvalues obtained from PCA motion models generated from all treatment fractions for Patient #1. As can be seen from the figure, the eigenvalues decrease with higher eigenmodes and they drop drastically after the third eigenmode in all treatment days. This may indicate that the higher eigenmodes contain minimal variance compared to the first ones. Figure 2 (b) shows the explained variance ratio for each eigenvector. In this figure, the individual explained variance and the cumulative explained variance are shown. As can be seen from the figure, most of the variance (79.32% of the variance) can be explained by the first eigenvector alone. The second eigenvector still holds some information (14.60% of the variance), while the third and the fourth principal components contain 3.20% and 2.41% of the variance, respectively. In this case, the first two eigenvectors together contain about 94% of the information (i.e., explain 94% of the variance).

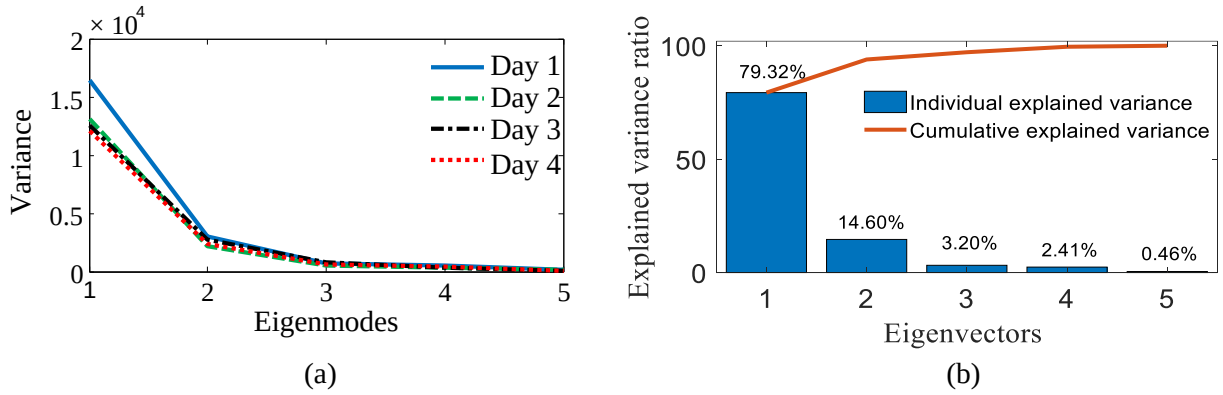

Figure 2: Variance explained by eigenvectors. (a) Eigenvalues' spectrum of the motion models of Patient #1 over a treatment course. (b) Explained variance ratio of the motion model of Patient #1 at Day 1.

In the following Sections 3.A – 3.C, the day-to-day variations of the motion models built from each fraction of treatment are presented. The evaluation criteria discussed in Section 2.C is applied on all the eigenmodes resulted from applying PCA on the DVF dataset (five in this study) to give the reader insights about the variability and stability of all eigenvectors of PCA motion models built from subsequent fractions of treatment. The results are discussed and compared to relevant studies in the field in Section 4.

3.A. Root mean square (RMS) difference

In this section, the RMS difference between the eigenvectors of the first fraction and the corresponding eigenvectors in the subsequent fractions is quantified. Figure 3 shows the average RMS differences for all patient datasets used in this study at different eigenmodes considering both alignment cases. As can be seen from the figure, the RMS difference between the eigenvectors of the motion model derived from the first fraction and the corresponding eigenvectors in the subsequent fractions increases with the higher eigenmodes in both alignment cases. For higher eigenmodes, the RMS difference between the eigenvectors in the first fraction and the eigenvectors in the subsequent fractions remained unchanged in both alignment cases. This may indicate that the eigenvectors at higher eigenmodes (4 and 5) have minimal variance and may only contain random information that has no useful implications on the organ motion represented by the DVFs.

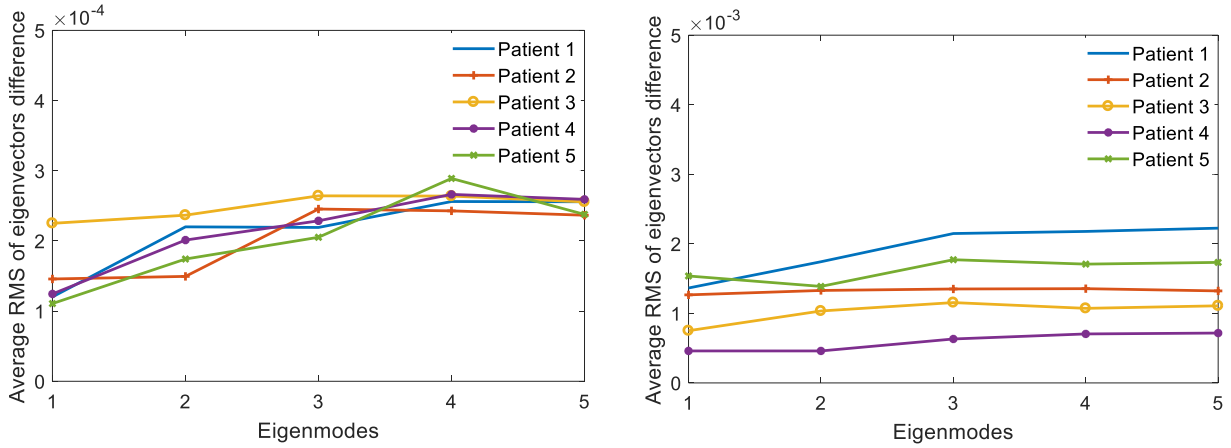

Figure 3: The average RMS difference between the eigenvectors of the reference motion model derived from the first fraction and the corresponding eigenvectors of the motion models derived from subsequent fractions for all patient datasets at each eigenmode, considering two alignment cases: (a) Alignment #1 uses rigid registration with respect to bony anatomy and (b) Alignment #2 uses rigid registration with respect to an ROI around the tumor, as defined in Section 2.C.b.

3.B. Directional similarity

In this section, the directional similarity between eigenvectors of the first fraction and the eigenvectors of the subsequent fractions is measured. Table 1 shows the average dot product between the eigenvectors of the motion model derived from the first fraction and the eigenvectors derived from all other fractions at each eigenmode for all datasets. The results in Table 1 are under Alignment #1. As seen in Table 1, the dot product decreases with higher eigenmodes, i.e., corresponding eigenvecors at the first few eigenmodes have more similarities in direction than those at the higher eigenmodes.

Table 1: Average dot product between the eigenvectors of the motion model derived from the first fraction and the corresponding eigenvectors of the motion models derived from subsequent fractions for all patient datasets under Alignment #1.

Eigenmodes	Patient 1	Patient 2	Patient 3	Patient 4	Patient 5	Average
1	0.777	0.669	0.294	0.754	0.811	**0.661**
2	0.192	0.653	0.229	0.371	0.532	**0.395**
3	0.255	0.063	-0.018	0.172	0.351	**0.165**
4	-0.013	0.076	-0.100	-0.096	-0.288	**-0.084**
5	-0.011	0.137	-0.016	-0.036	0.129	**0.041**

Table 2 shows the average dot product between the eigenvectors of the motion model derived from the first fraction and the eigenvectors in the subsequent fraction at each eigenmode for all datasets under Alignment #2.

Table 2: Average dot product between the eigenvectors of the motion model derived from the first fraction and the corresponding eigenvectors of the motion models derived from subsequent fractions for all patient datasets under Alignment #2.

Eigenmodes	Patient 1	Patient 2	Patient 3	Patient 4	Patient 5	Average
1	0.619	0.143	0.542	0.542	0.387	**0.446**
2	0.380	0.001	0.128	0.571	0.305	**0.277**
3	0.081	-0.050	-0.074	0.266	-0.043	**0.036**
4	0.056	-0.018	0.081	0.081	-0.033	**0.033**
5	0.015	0.002	0.019	0.055	-0.020	**0.014**

Table 2 showed that the first few eigenmodes typically had larger dot products than the last few ones. The dot product decreases with higher eigenmodes, which also indicates that corresponding eigenvecors at the first few eigenmodes have more similarities in direction than those at the higher eigenmodes. The clinical relevance of these results are discussed in Section 4.

3.C. Euclidean Model Norm

The EMN evaluates how well an eigenvector in the subsequent fractions can be represented by a motion model derived from a reference fraction. EMN evaluation metric has been described in Section 2.C.a. Table 3 shows the average EMN between the motion model formed by the first three eigenvectors of the first fraction and all other eigenvectors in the subsequent fractions for all datasets under Alignment #1. As shown in Table 3, EMN decreases with higher eigenmodes.

Table 3: The average EMN between the motion model formed by the first three eigenvectors of the first fraction and all other eigenvectors in the subsequent fractions in all patient datasets under Alignment #1.

Eigenmodes	Patient 1	Patient 2	Patient 3	Patient 4	Patient 5	Average
1	0.804	0.757	0.674	0.776	0.819	**0.766**
2	0.531	0.718	0.595	0.549	0.554	**0.589**
3	0.349	0.209	0.204	0.371	0.426	**0.312**
4	0.316	0.110	0.126	0.320	0.123	**0.199**
5	0.063	0.118	0.128	0.196	0.117	**0.124**

Similarly, Table 4 shows the average EMN between the motion model formed by the first three eigenvectors of the first fraction and all other eigenvectors in the subsequent fractions for all datasets under Alignment #2.

Table 4: The average EMN between the motion model formed by the first three eigenvectors of the first fraction and all other eigenvectors in the subsequent fractions in all patient datasets under Alignment #2.

Eigenmodes	Patient 1	Patient 2	Patient 3	Patient 4	Patient 5	Average
1	0.735	0.502	0.544	0.821	0.835	**0.687**
2	0.609	0.517	0.332	0.736	0.668	**0.572**
3	0.414	0.347	0.369	0.405	0.335	**0.374**
4	0.258	0.185	0.252	0.241	0.167	**0.220**
5	0.336	0.199	0.148	0.121	0.237	**0.208**

Table 3 and Table 4 show the same trend where the EMN decreases with higher eigenmodes. To summarize the results, the average RMS, directional similarity (dot product), and EMN of the first two eigenvectors are calculated and compared to those of the last three eigenvectors. Results showed that the eigenvectors at the first two eigenmodes have smaller RMS (0.00017), larger dot product (0.528), and larger EMN (0.678) than those at higher eigenmodes (RMS: 0.00025, dot product: 0.041, and EMN: 0.212) considering Alignment #1.

Figure 4 shows the result of applying the evaluation criteria used in this paper (i.e., RMS, dot product, and EMN) on a sample patient underwent a five-day radiotherapy course. In this figure, the variations between the eigenvectors of the reference motion model derived from the first fraction and the corresponding motion models derived from the subsequent fractions are demonstrated at each eigenmode across fractions. As can be seen from the plots in Figure 4, the inter-fraction differences between the reference motion model and the subsequent ones are noticed in all fractions, even among the first few eigenmodes. However, there is no time trend noticed. These results are in agreement with the results obtained in Figure 3 and Tables 1- 4 where the eigenvectors at the first (2-3) eigenmodes remained the most stable, having smaller RMS, larger dot product, and larger EMN than those at higher eigenmodes. The relative standard deviation in RMS across fractions was no more than 3.5% for the first three eigenmodes. It did not exceed 12% in dot product (1.6%, 5.8%, and 12% for the first, second, and third eigenmodes, respectively), and 15% in EMN (1.4%, 7.8%, and 15% for the first, second, and third eigenmodes, respectively).

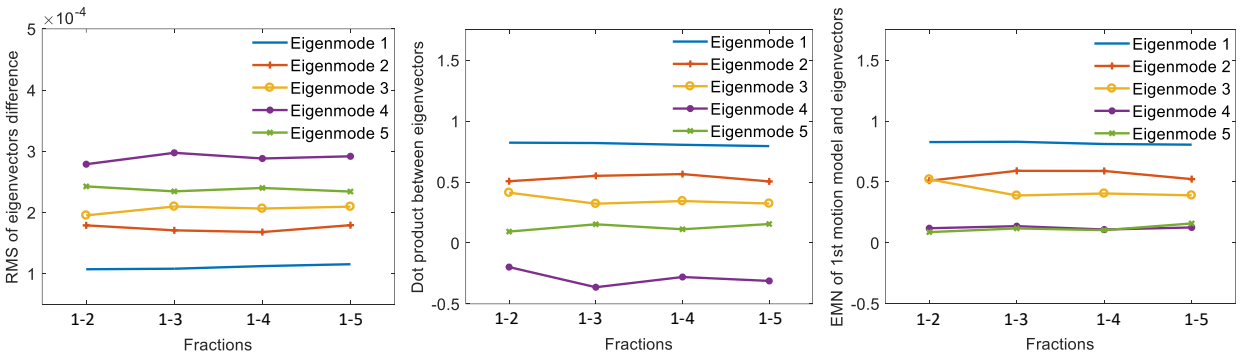

Figure 4: The evaluation metrics applied on the eigenvectors of the reference motion model derived from the first fraction and the corresponding eigenvectors derived from subsequent fractions at each eigenmode for Patient #5 under Alignment #1. Metrics are: (a) RMS difference, (b) dot product, and (c) EMN between the motion model formed by the first three eigenvectors of the first fraction and all other eigenvectors in the subsequent fractions.

4. Discussion

In this work, the variations of motion models derived from several fractions of a radiotherapy treatment course have been measured based on different criteria: 1) the RMS differences between the eigenvectors of the motion model derived from the first fraction and the corresponding eigenvectors of subsequent fractions, 2) the directional similarity calculated as the dot product between the eigenvectors of the motion model derived from the first fraction and the corresponding eigenvectors of subsequent fractions, and 3) the EMN

between a motion model formed by the first three eigenvectors of the first fraction and every eigenvector in the subsequent fractions. The criteria is measured on sets of images considering two alignment settings where: 1) the entire 4DCBCT images in the subsequent fractions are registered using rigid registration with respect to the bony anatomy to the corresponding 4DCBCT images in the first fraction (Alignment #1), and 2) the entire 4DCBCT images in the subsequent fractions are registered using rigid registration with respect to an ROI around the tumor in the 4DCBCT images in the first fraction (Alignment #2).

Results showed that the first eigenvectors (associated with the largest eigenvalues) contain more variance than the eigenvectors at higher eigenmodes, as depicted in Figure 2 (a). The individual explained variance and the cumulative explained variance plotted in Figure 2 (b) showed that most of the variance in the DVF dataset was explained by the first 2-3 eigenvectors. This may indicate that the rest of the eigenvectors can be dropped safely without losing important information. This may also support the findings of other studies that have shown that a motion model built from the first 2-3 eigenvectors was able to fully represent organ motion extracted in the DVFs [5], [37].

RMS represents an absolute difference between the values of the corresponding eigenvectors. It was noticed that the RMS difference between the corresponding eigenvectors increases with higher eigenmodes in both alignment cases as seen in Figure 3. This indicates that the eigenvectors in the first few eigenmodes are more stable and represent similar motion to the reference motion model than the ones at higher eigenmodes. The eigenvectors at higher eigenmodes (4 and 5) showed no increase in RMS which may indicate that these eigenvectors only contain random information that will not contribute to the motion model. In Figure 3 (b), the RMS is calculated from datasets after using rigid registration of an ROI around the tumor (Alignment #2). The larger scale gives an indication that the RMS differences (absolute distance) between these eigenvectors are larger. Having an ROI around soft tissues may increase the difference between the bone alignment (especially if the tumor is localized adjacent to the bone), and this may increase the difference between the eigenvectors of the different fractions. The RMS has some limitations as it results in a single number calculated from all vectors in the DVFs including the DVFs representing the motion of image areas that are not clinically of interest. Thus, RMS is not used in this study as a standalone evaluation metric to evaluate the day-to-day variations of motion models. However, it can be useful to understand the behavior of the motion vectors across fractions.

The values of the dot product between any two eigenvectors can indicate the directional similarity between them. The purpose of using this metric is to measure the directional similarity between the eigenvectors of the reference motion model derived from the first fraction and the eigenvectors of motion models derived from subsequent fractions. Low values of dot product, i.e. below or around zero, for eigenvectors at specific eigenmodes across fractions may indicate that these eigenvectors cannot be used to represent a reliable motion model. Using the dot product as an evaluation measure between the eigenvectors, it is noticed that the directional similarity between the eigenvectors of the first fraction and their correspondences in subsequent fractions decreases with higher eigenmodes. Eigenvectors at higher eigenmodes show no similarity to those at the first reference motion model which may indicate that these eigenvectors may only contain noise. The higher directional similarity seen between the eigenvectors at the first few eigenmodes can imply that a reference motion model formed by these eigenvectors can have higher stability, therefore can represent the organ motion variations through a treatment course, which we are further investigating using the EMN metric introduced in this paper.

The EMN metric was intended to be used as a global measure to evaluate how effectively a set of eigenvectors from the first fraction can represent the organ motion in the subsequent fractions. We chose the first three eigenvectors from the first fraction because, as shown by the explained variance plot depicted in Figure 2, we anticipate that the PCA sorts the eigenvectors by the amount of variance they can describe in the dataset and thus can be used to represent the motion patterns in the subsequent fractions (i.e., the first three eigenvectors form the reference motion model). This criteria can also estimate how much information can be lost if the motion model built from the first fraction is used in the subsequent treatment days. Results showed that EMN values decrease with higher eigenmodes. This may indicate that only the first few eigenvectors in the subsequent fractions can be represented by a reference motion model formed by the first three eigenvectors obtained from the reference fraction.

According to the results obtained using all the evaluation metrics considering two alignment cases, it has been noticed that Alignment #1 resulted in less variability between the reference fraction and the subsequent fractions compared to Alignment #2. This indicates that image registration with respect to an ROI around soft-tissues may increase the difference between the bone alignment in the images which may result in increasing the difference between the eigenvectors at the different fractions. Thus, according to our results, rigid registration with respect to bony anatomy between fractions may be preferred when dealing with PCA motion models or other motion models that involve using motion displacement vectors.

Using the three metrics discussed in this study, the clinical implications of our findings are summarized as follows:

(1) Lung motion at each fraction of the 4DCBCT datasets can be completely represented by 2-3 eigenvectors.

(2) A single reference motion model derived from the first few (2-3) eigenvectors from the first fraction may stay stable and reliable to represent the motion in the subsequent fractions.

(3) Variances are still seen even in the first few PCA eigenvectors on a day-to-day basis. Quantifying the effect of these variations on the motion reconstruction accuracy need to be studied for specific clinical tasks.

(4) Applying rigid registration according to bony anatomy on the entire 4DCBCT images in the subsequent fractions to align them to the entire images in the first fraction may reduce the day-to-day variations in PCA eigenvectors.

The clinical importance of studying the inter-fraction variability of PCA motion model is not limited to the ability of using one motion model to represent the entire lung motion through several fractions. Incremental motion modeling techniques can be derived to update/enhance the reference motion model to include additional motion variations that were not known in the reference motion model. Moreover, other imaging techniques may contribute to update the reference patient-specific motion model. The work presented in this paper can be useful in clinical applications such as 4D dose accumulation or tumor tracking. For tumor tracking, having knowledge of the day-to-day variations in patient anatomy or motion patterns can be useful in verifying the position of the tumor and normal structures during radiotherapy treatment delivery [8]. Also the motion models estimated from each fraction can be used to estimate and/or verify the delivered dose distributions [38], [39]. 4DCBCT-based motion models are used to generate 3D time-varying images [17]. 3D fluoroscopic images may be more accurate if estimated at each treatment fraction than using the planning 4DCT images or the 4DCBCT images of the first treatment fraction to derive the motion model, especially when there are uncertainties in the setup, tumor position or respiratory motion pattern, between simulation and treatment, or changes in the patient anatomy. However,

using 4DCBCT images to estimate motion models can present other challenges that make dose calculation difficult such as the poor quality of the 4DCBCT images used in building the motion model. One cause of poor image quality in 4DCBCT volumes is having too few projections for image reconstruction.

It is important to discuss other sources of uncertainty that may cause variations in motion models other than the actual day-to-day variations. First, the accuracy of the PCA motion models depends on the accuracy of the 4DCBCT images that are used to build the models. Second, the DIR algorithm applied to these images may also introduce inaccuracies or uncertainties. Both image and motion artifacts in 4DCBCT are likely to degrade the quality of DIR. PCA as a dimensionality reduction method is able to remove small independent noise in the DVFs generated by DIR methods but it is does not eliminate large errors in the deformation [8]. Li et al. studied the contribution of the error produced by the PCA motion model derived from 4DCT image datasets on the tumor localization error in the generated 3D time-varying images [8]. Their study showed that the error introduced by the PCA lung motion model is insignificant comparing to the error produced by the 2D/3D registration used in that work. Similarly, Dhou et al. studied the effect of the undersampling of 4DCBCT data on tumor localization in the generated 3D time-varying images using PCA motion models and 3D registration [17]. Their study showed that the error in tumor localization was around 3 times larger using a severely undersampled data set than using a well-sampled one. In this work, the 4DCBCT images used to build the model suffer from the poor quality because of the too few projections used to reconstruct these images. The streaking artifacts in these images may have contributed to degrade the quality of DIR which subsequently affected the PCA motion models built based on the resulting DVFs. Various methods have been proposed to address the undersampling problem and to improve image quality in 4DCBCT, such as compressed sensing [19]–[23], motion compensated reconstruction [24], [40]–[42], intermediate frame interpolation [43]–[47], and other advanced methods [48], [49]. Future studies may consider these methods to improve 4DCBCT images before using them in building motion models. Day-to-day variations may also be studied using these improved 4DCBCT images and compared to the findings of this study.

5. Conclusion

This paper presented a quantitative evaluation of the day-to-day variations of PCA motion models built from 4DCBCT images. The experiments and analysis was performed on five patient datasets each with multiple treatment fractions. The findings of this study supported the findings of other relevant studies in the assumption that lung motion at a specific treatment day can be completely represented by 2-3 eigenvectors. The study also showed that the first few eigenvectors (2-3) of the PCA motion model remained the most stable (similar to those of the reference model built from the first fraction images) over a course of radiotherapy treatment. For a sample patient, the RMS, dot product, and EMN did not vary more than 3.5%, 12%, and 15%, respectively across five fractions for the first three eigenmodes. Thus, a motion model built from the first few PCA eigenvectors can represent the patient motion during a radiotherapy treatment course. Despite their relatively greater stability, day-to-day variations are still noticed among the first few motion model eigenvectors. The study also found that registering the entire 4DCBCT images in the subsequent fractions to the entire images in the first fraction with respect the bony anatomy may reduce the day-to-day variations in PCA eigenvectors. In future work, the effect of these day-to-day variations on motion modeling applications will be investigated for target localization and dose calculation.

Acknowledgement

This project was supported, in part, through a Master Research Agreement with Varian Medical Systems, Inc., Palo Alto, CA. The authors have no relevant conflicts of interest to disclose.

References

[1] K. Matsugi *et al.*, "Measurement of Interfraction Variations in Position and Size of Target Volumes in Stereotactic Body Radiotherapy for Lung Cancer," *Int. J. Radiat. Oncol. Biol. Phys.*, vol. 75, no. 2, pp. 543–548, 2009.

[2] P. J. Keall *et al.*, "The management of respiratory motion in radiation oncology report of AAPM Task Group 76," *Med Phys*, vol. 33, no. 10, pp. 3874–3900, 2006.

[3] M. Sohn, M. Birkner, D. Yan, and M. Alber, "Modelling individual geometric variation based on dominant eigenmodes of organ deformation: implementation and evaluation," *Phys Med Biol*, vol. 50, no. 24, pp. 5893–5908, 2005.

[4] Q. Zhang *et al.*, "A patient-specific respiratory model of anatomical motion for radiation treatment planning.," *Med. Phys.*, vol. 34, no. 12, pp. 4772–4781, 2007.

[5] R. Li *et al.*, "Real-time volumetric image reconstruction and 3D tumor localization based on a single x-ray projection image for lung cancer radiotherapy," *Med Phys*, vol. 37, no. 6, pp. 2822–2826, 2010.

[6] Q. Zhang, Y. C. Hu, F. Liu, K. Goodman, K. E. Rosenzweig, and G. S. Mageras, "Correction of motion artifacts in cone-beam CT using a patient-specific respiratory motion model," *Med Phys*, vol. 37, no. 6, pp. 2901–2909, 2010.

[7] A. Fassi, J. Schaerer, M. Fernandes, M. Riboldi, D. Sarrut, and G. Baroni, "Tumor tracking method based on a deformable 4D CT breathing motion model driven by an external surface surrogate," *Int J Radiat Oncol Biol Phys*, vol. 88, no. 1, pp. 182–188, 2014.

[8] R. Li *et al.*, "3D tumor localization through real-time volumetric x-ray imaging for lung cancer radiotherapy," *Med Phys*, vol. 38, no. 5, pp. 2783–2794, 2011.

[9] M. Hurwitz *et al.*, "Generation of fluoroscopic 3D images with a respiratory motion model based on an external surrogate signal," *Phys. Med. Biol.*, vol. 60, no. 2, 2015.

[10] M. Van Herk, L. Zijp, P. Remeijer, J. Wolthaus, and J. J. Sonke, "On-line 4D cone beam CT for daily correction of lung tumour position during hypofractionated radiotherapy," *ICCR, Toronto, Canada*, 2007.

[11] M. Guo *et al.*, "Reconstruction of a high-quality volumetric image and a respiratory motion model from patient CBCT projections," *Med. Phys.*, 2019.

[12] P. Mishra *et al.*, "Evaluation of 3D fluoroscopic image generation from a single planar treatment image on patient data with a modified XCAT phantom," *Phys Med Biol*, vol. 58, no. 4, pp. 841–858, 2013.

[13] L. Zijp, J.-J. Sonke, and M. van Herk, "Extraction of the respiratory signal from sequential thorax cone-beam X-ray images," in *International Conference on the Use of Computers in Radiation Therapy*, 2004, pp. 507–509.

[14] J. J. Sonke, L. Zijp, P. Remeijer, and M. van Herk, "Respiratory correlated cone beam CT," *Med Phys*, vol. 32, no. 4, pp. 1176–1186, 2005.

[15] S. Dhou, Y. Motai, and G. D. Hugo, "Local intensity feature tracking and motion modeling for respiratory signal extraction in cone beam CT projections," *IEEE Trans. Biomed. Eng.*, vol. 60, no. 2, pp. 332–342, 2013.

[16] S. Dhou, A. Docef, and G. Hugo, "Image-based respiratory signal extraction using dimensionality reduction for phase sorting in Cone-Beam CT Projections," in *ACM International Conference Proceeding Series*, 2017.

[17] S. Dhou *et al.*, "3D fluoroscopic image estimation using patient-specific 4DCBCT-based motion models," *Phys Med Biol*, vol. 60, no. 9, pp. 3807–24, 2015.

[18] S. Dhou, M. Hurwitz, P. Mishra, R. Berbeco, and J. Lewis, "4DCBCT-based motion modeling and 3D fluoroscopic image generation for lung cancer radiotherapy," in *Progress in Biomedical Optics and Imaging - Proceedings of SPIE*, 2015, vol. 9415.

[19] G. H. Chen, J. Tang, and S. Leng, "Prior image constrained compressed sensing (PICCS): a method to accurately reconstruct dynamic CT images from highly undersampled projection data sets," *Med Phys*, vol. 35, no. 2, pp. 660–663, 2008.

[20] E. Y. Sidky and X. Pan, "Image reconstruction in circular cone-beam computed tomography by constrained, total-variation minimization," *Phys Med Biol*, vol. 53, no. 17, pp. 4777–4807, 2008.

[21] E. Y. Sidky, Y. Duchin, X. Pan, and C. Ullberg, "A constrained, total-variation minimization algorithm for low-intensity x-ray CT," *Med Phys*, vol. 38 Suppl 1, p. S117, 2011.

[22] H. Gao, R. Li, Y. Lin, and L. Xing, "4D cone beam CT via spatiotemporal tensor framelet," *Med Phys*, vol. 39, no. 11, pp. 6943–6946, 2012.

[23] K. Choi, L. Xing, A. Koong, and R. Li, "First study of on-treatment volumetric imaging during respiratory gated VMAT," *Med Phys*, vol. 40, no. 4, p. 40701, 2013.

[24] T. Li *et al.*, "Four-dimensional cone-beam computed tomography using an on-board imager," *Med Phys*, vol. 33, no. 10, pp. 3825–3833, 2006.

[25] A. M. Badawi, E. Weiss, W. C. th Sleeman, C. Yan, and G. D. Hugo, "Optimizing principal component models for representing interfraction variation in lung cancer radiotherapy," *Med Phys*, vol. 37, no. 9, pp. 5080–5091, 2010.

[26] A. M. Badawi, E. Weiss, W. C. Sleeman IV, and G. D. Hugo, "Classifying geometric variability by dominant eigenmodes of deformation in regressing tumours during active breath-hold lung cancer radiotherapy," *Physics in Medicine and Biology*, vol. 57, no. 2. pp. 395–413, 2011.

[27] G. Hugo, C. Vargas, J. Liang, L. Kestin, J. W. Wong, and D. Yan, "Changes in the respiratory pattern during radiotherapy for cancer in the lung," *Radiother. Oncol.*, vol. 78, no. 3, pp. 326–331, 2006.

[28] T. Juhler Nøttrup *et al.*, "Intra- and interfraction breathing variations during curative radiotherapy for lung cancer," *Radiother. Oncol.*, vol. 84, no. 1, pp. 40–48, 2007.

[29] K. J. Redmond, D. Y. Song, J. L. Fox, J. Zhou, C. N. Rosenzweig, and E. Ford, "Respiratory Motion Changes of Lung Tumors Over the Course of Radiation Therapy Based on Respiration-Correlated Four-Dimensional Computed Tomography Scans," *Int. J. Radiat. Oncol. Biol. Phys.*, vol. 75, no. 5, pp. 1605–1612, 2009.

[30] J. J. Sonke, J. Lebesque, and M. van Herk, "Variability of Four-Dimensional Computed Tomography Patient Models," *Int. J. Radiat. Oncol. Biol. Phys.*, vol. 70, no. 2, pp. 590–598, 2008.

[31] S. Rit, M. Van Herk, L. Zijp, and J. J. Sonke, "Quantification of the variability of diaphragm motion and implications for treatment margin construction," *Int. J. Radiat. Oncol. Biol. Phys.*, vol. 82, no. 3, 2012.

[32] S. Dhou, D. Ionascu, C. Williams, and J. Lewis, "Inter-fraction variations in motion modeling using patient 4D-cone beam CT images," in *2018 Advances in Science and Engineering Technology International Conferences, ASET 2018*, 2018, pp. 1–4.

[33] L. A. Feldkamp, L. C. Davis, and J. W. Kress, "Practical cone-beam algorithm," *J. Opt. Soc. Am. A Opt. Image Sci. Vis.*, vol. 1, no. 6, pp. 612–619, 1984.

[34] S. Rit, M. Vila Oliva, S. Brousmiche, R. Labarbe, D. Sarrut, and G. C. Sharp, "The Reconstruction Toolkit (RTK), an open-source cone-beam CT reconstruction toolkit based on the Insight Toolkit (ITK)," in *International Conference on the Use of Computers in Radiation Therapy (ICCR'13)*, 2013.

[35] X. Gu *et al.*, "Implementation and evaluation of various demons deformable image registration algorithms on a GPU," *Phys Med Biol*, vol. 55, no. 1, pp. 207–219, 2010.

[36] R. Li *et al.*, "On a PCA-based lung motion model.," *Phys. Med. Biol.*, vol. 56, no. 18, pp. 6009–6030, 2011.

[37] S. Dhou *et al.*, "3D fluoroscopic image estimation using patient-specific 4DCBCT-based motion models," *Phys. Med. Biol.*, vol. 60, no. 9, 2015.

[38] W. Cai *et al.*, "3D delivered dose assessment using a 4DCT-based motion model," *Med. Phys.*, vol. 42, no. 6, pp. 2897–2907, 2015.
[39] W. Cai *et al.*, "4D cone beam CT-based dose assessment for SBRT lung cancer treatment," *Phys. Med. Biol.*, vol. 61, no. 2, pp. 554–568, 2016.
[40] T. Li, A. Koong, and L. Xing, "Enhanced 4D cone-beam CT with inter-phase motion model," *Med Phys*, vol. 34, no. 9, pp. 3688–3695, 2007.
[41] S. Rit, J. Wolthaus, M. van Herk, and J. J. Sonke, "On-the-fly motion-compensated cone-beam CT using an a priori motion model," *Med Image Comput Comput Assist Interv*, vol. 11, no. Pt 1, pp. 729–736, 2008.
[42] S. Rit, D. Sarrut, and L. Desbat, "Comparison of analytic and algebraic methods for motion-compensated cone-beam CT reconstruction of the thorax," *IEEE Trans Med Imaging*, vol. 28, no. 10, pp. 1513–1525, 2009.
[43] G. H. Weiss, A. J. Talbert, and R. A. Brooks, "The use of phantom views to reduce CT streaks due to insufficient angular sampling," *Phys Med Biol*, vol. 27, no. 9, pp. 1151–1162, 1982.
[44] T. M. Lehmann, C. Gonner, and K. Spitzer, "Addendum: B-spline interpolation in medical image processing," *IEEE Trans Med Imaging*, vol. 20, no. 7, pp. 660–665, 2001.
[45] T. Li, E. Schreibmann, Y. Yang, and L. Xing, "Motion correction for improved target localization with on-board cone-beam computed tomography," *Phys Med Biol*, vol. 51, no. 2, pp. 253–267, 2006.
[46] M. Bertram, J. Wiegert, D. Sch??fer, T. Aach, and G. Rose, "Directional view interpolation for compensation of sparse angular sampling in cone-beam CT," *IEEE Trans. Med. Imaging*, vol. 28, no. 7, pp. 1011–1022, 2009.
[47] S. Dhou, G. D. Hugo, and A. Docef, "Motion-based projection generation for 4D-CT reconstruction," in *Proceedings of the IEEE International Conference on Image Processing (ICIP)*, 2014, pp. 1698–1702.
[48] X. Jia, Z. Tian, Y. Lou, J. J. Sonke, and S. B. Jiang, "Four-dimensional cone beam CT reconstruction and enhancement using a temporal nonlocal means method," *Med Phys*, vol. 39, no. 9, pp. 5592–5602, 2012.
[49] J. Wang and X. Gu, "High-quality four-dimensional cone-beam CT by deforming prior images," *Phys Med Biol*, vol. 58, no. 2, pp. 231–246, 2013.